Monitoring surface currents from uncertain image observations

Isabelle Herlin, Etienne Huot

1. Introduction

The paper discusses the estimation of surface motion from satellite acquisitions of Black Sea. Estimating motion from an image sequence is still intensively studied in the literature. A recent survey of research performed in the image processing community, concerning fluid flow observations, can be found in (Heitz et al., 2010). Application of data assimilation methods, in order to solve this problem, emerged around five-six years ago. Unlike most image processing methods, which apply a Tikhonov regularisation in order to solve motion's aperture problem, data assimilation relies on a dynamic model of apparent velocity. Readers can refer to (Papadakis et al., 2007), (Titaud et al., 2010), and (Béréziat and Herlin, 2011) for recent contributions to the subject. However, the dynamic model is also uncertain and only approximates the processes, that are underlying the image evolution.

The model, that is used in the paper for motion estimation, includes the Lagrangian constancy of velocity and expresses the transport of image brightness by the motion field. Image assimilation allows an estimation of motion, based on the uncertainties of image data and model, that are translated as error terms in equations. The paper discusses both issues:

- Uncertain image information. This requires the definition of dedicated observation operators and observation errors, in order to optimize the estimation process.
- Uncertain model. This requires the involvement of a model error. A weak 4D-Var is described in order to estimate motion. Improvements obtained, when including this error in the control, are discussed and analyzed.

Results are quantified on synthetic images and illustrated on satellite data, acquired over Black Sea by NOAA-AVHRR sensors. Perspectives of the research concern the short-term prediction of surface currents on the whole basin.

Section 2 provides the mathematical setting of the paper and describes the data assimilation method, that is applied to retrieve surface motion from an image sequence. The issue of the choice of image information, to be involved in the estimation, and that of model error are discussed in Section 3. Section 4 quantifies and analyses results, and conclusions and perspectives are given in Section 5.

2. Problem statement

Let us denote Ω the bounded domain, corresponding to image acquisitions, $[0, t_f]$ the temporal domain, on which images are acquired, and $A = \Omega \times [0, t_f]$. $\mathbf{x} = (x, y)^T$ denotes the position of a pixel in the image domain and t the temporal index.

Let $I(t)$ denotes the continuous image sequence, providing the discrete acquired sequence I_i, $1 < \cdots < i < \cdots < N_{\text{obs}}$, that is processed in order to estimate motion.

The assumption, that is used to define the dynamic model, is the Lagrangian constancy of the motion vector, $\frac{d\mathbf{w}}{dt} = 0$, with $\mathbf{w} = \begin{pmatrix} u & v \end{pmatrix}^T$ the motion vector, and u and v its zonal

and meridional components. According to that assumption, the velocity is constant along each pixel's trajectory. This is rewritten as :

$$\frac{du}{dt} = 0 \Leftrightarrow \frac{\partial u}{\partial t} + u\frac{\partial u}{\partial x} + v\frac{\partial u}{\partial y} = 0 \tag{1}$$

$$\frac{dv}{dt} = 0 \Leftrightarrow \frac{\partial v}{\partial t} + u\frac{\partial v}{\partial x} + v\frac{\partial v}{\partial y} = 0 \tag{2}$$

We define a pseudo-image $I_s(\mathbf{x}, t)$, that is transported by surface velocity $\mathbf{w}(\mathbf{x}, t)$, with the same heuristics as the image sequence: this is the optical flow constraint equation (Horn and Schunk, 1981), expressed as:

$$\frac{\partial I_s}{\partial t} + \nabla I_s.\mathbf{w} = 0 \tag{3}$$

These pseudo-images will be directly compared to satellite images, during the estimation process. They will be forced to be almost identical at acquisition dates.

The state vector $\mathbf{X}$ is defined as $\begin{pmatrix} u & v & I_s \end{pmatrix}^T$, on the space-time domain A. The 4D-Var algorithm estimates motion from image acquisitions by solving the following system of three equations :

$$\begin{aligned} \frac{\partial \mathbf{X}}{\partial t}(\mathbf{x}, t) + \mathbb{M}(\mathbf{X})(\mathbf{x}, t) &= 0 & (4)\\ \mathbf{X}(\mathbf{x}, 0) - \mathbf{X}_b(\mathbf{x}) &= \epsilon_B(\mathbf{x}) & (5)\\ \mathbb{H}(\mathbf{X}, I)(\mathbf{x}, t) &= \epsilon_R(\mathbf{x}, t) & (6) \end{aligned}$$

The first one is the so-called evolution equation, that summarizes Eqs. (1), (2) and (3). One can notice that $\mathbf{X}(\mathbf{x}, t)$, for any t, is only determined from $\mathbf{X}(\mathbf{x}, 0)$ and the integration of Equation (4).

Equation (5) corresponds to the knowledge, that is usually available on the state vector at initial date 0, and expressed as the background value $\mathbf{X}_b(\mathbf{x})$. The solution, estimated by the 4D-Var algorithm, should stay close to this background value. However, as this knowledge is uncertain, an error term, $\epsilon_B(\mathbf{x})$, is added to the equation. For motion estimation, no information is available on the initial value of the velocity field, and its initialization value is null, while the background on the pseudo-image I_s is the first image of the sequence I_1. The background equation is then simplified as a scalar equation:

$$\mathbb{P}(\mathbf{X}(\mathbf{x}, 0)) - I_1(\mathbf{x}) = \epsilon_B(\mathbf{x}) \tag{7}$$

where $\mathbb{P}$ is the projection on the pseudo-image component.

Last, Equation (6) is named observation equation. It links the image observations I to the state vector $\mathbf{X}$. In this case, $\mathbb{H}$ denotes the observation operator, that compares the pseudo-image I_s to image observations. They have to be almost identical and the observation equation is also scalar:

$$\mathbb{H}(\mathbf{X}, I)(\mathbf{x}, t) = \mathbb{P}(\mathbf{X}(\mathbf{x}, t)) - I(\mathbf{x}, t) = \epsilon_R(\mathbf{x}, t) \tag{8}$$

The discrepancy between pseudo-images and observations is described by the error term $\epsilon_R(\mathbf{x}, t)$.

In the context of variational data assimilation, the error terms $\epsilon_B(\mathbf{x})$ and $\epsilon_R(\mathbf{x}, t)$ are supposed Gaussian and zero-mean. We additionaly suppose no correlation in space and time. The respective variance values are written $B(\mathbf{x})$ and $R(\mathbf{x}, t)$.

Solving System (4, 7, 8) is then written as a minimisation problem. The objective is to find the minimum $\mathbf{X}(0)$ of the cost function J:

$$J(\mathbf{X}(0)) = \frac{1}{2}\int_A \frac{(\epsilon_R(\mathbf{x},t))^2}{R(\mathbf{x},t)}d\mathbf{x}dt + \frac{1}{2}\int_\Omega \frac{(\epsilon_B(\mathbf{x}))^2}{B(\mathbf{x})}d\mathbf{x} \tag{9}$$

According to (Le Dimet and Talagrand, 1986), let λ be the adjoint variable, defined as the solution of Equations (10) and (11):

$$\lambda(t_f) = 0 \tag{10}$$

$$-\frac{\partial\lambda(t)}{\partial t} + \left(\frac{\partial\mathbb{M}}{\partial\mathbf{X}}\right)^* \lambda(t) = \mathbb{P}^T\left(\frac{\mathbb{P}(\mathbf{X}(\mathbf{x},t) - I(\mathbf{x},t)}{R(\mathbf{x},t)}\right) \tag{11}$$

The adjoint model $\frac{\partial\mathbb{M}}{\partial\mathbf{X}}^*$ verifies the definition of an adjoint operator:

$$\int \left(\frac{\partial\mathbb{M}}{\partial\mathbf{X}}(\eta)\right)^T \lambda d\mu = \int \eta^T \left(\frac{\partial\mathbb{M}}{\partial\mathbf{X}}\right)^* (\lambda) d\mu \tag{12}$$

for all integrable functions η and λ. Le Dimet and Talagrand demonstrated that the gradient of J verifies:

$$\frac{\partial J}{\partial\mathbf{X}(0)} = \mathbb{P}^T\left(\frac{\mathbb{P}(\mathbf{X}(0)) - I_1}{B}\right) + \lambda(0) \tag{13}$$

Minimum of J is then obtained with a method of steepest descent and the L-BFGS algorithm (Zhu et al., 1997).

3. Uncertainties

This section is split in two parts. The first one discusses the uncertainty on the image data and the definition of image information, that has to be assimilated. The second one concerns the uncertainty on the evolution equation and the involvement of a model error.

3.1 Uncertainty on image information

Processing images and retrieving their motion field is a difficult issue, that faces a large range of practical and theorical problems.

In the case of satellite data, images are contaminated by noise and often strongly corrupted by cloud cover. For discarding such pixels during the estimation process, their contribution to the energy function J, Equation (9) should be small. Then, $R(\mathbf{x},t)$ should get a high value, almost infinite, on those points, that are characterized as not valid by the metadata provided simultaneously with satellite images. This idea has been used for instance in (Herlin et al., 2011) in order to recover missing data with an inpainting method: pseudo-images obtained by the assimilation process are a denoised version of the real acquisitions.

Another crucial issue concerns the information, that is assimilated to retrieve motion. From Equation (3), it can be seen that motion estimation is possible, only if the gradient norm is high enough and correctly estimated. This may potentially affect the correct determination of velocity for structures with low contrast, as the gradient is computed by finite differences during the numerical integration of (3). For that purpose, we proposed in (Béréziat and Herlin,

2012) to consider a new observation operator, $\mathbb{H}_2$, that links the state vector to the image acquisitions, whose definition is:

$$\mathbb{H}_2(\mathbf{X}, I)(\mathbf{x}, t) = \frac{I_{i+1}(\mathbf{x}) - I_i(\mathbf{x})}{\triangle t_i} + \nabla I_i^T(\mathbf{x})\mathbf{w}(\mathbf{x}, t_i) \tag{14}$$

and that is only computed at acquisition dates, with $\triangle t_i$ the time interval between the two frames i and $i+1$ and t_i the acquisition date of image i. ∇I_i is computed by efficient algorithms (See (Deriche, 1987)), that allow a good estimation of the gradient norm, even in case of a low constrast, and a good location of the contour points, which is mandatory for having structures correctly positioned in space. An error term is associated to that additional observation operator, denoted $\epsilon_{R2}(\mathbf{x}, t)$, with a variance value $R_2(\mathbf{x}, t)$. Last, a second term is added in the right part of the backward Equation (11), with the adjoint of $\mathbb{H}_2$ being equal to:

$$\left(\frac{\partial \mathbb{H}_2}{\partial \mathbf{X}}\right)^* (\mathbf{X})(\mathbf{x}, t_i) = \begin{pmatrix} \nabla I_i(\mathbf{x}) & 0 \end{pmatrix}^T \tag{15}$$

Improvements obtained thanks to that second observation operator are discussed in the results section.

3.2 Uncertainty on evolution laws

The heuristics on the dynamics of the image sequence, the transport equation, and those on the motion field, the Lagrangian constancy, are only a rough approximation of the reality. This would be the same for any mathematical model. This uncertainty on the geophysical processes underlying the image sequence requires the introduction of an error term $\epsilon(x, t)$ in the evolution equation, (Trémolet, 2006), (Valur Hólm, 2008), and (Herlin et al., 2012):

$$\frac{\partial \mathbf{X}}{\partial t}(x, t) + \mathbb{M}(\mathbf{X})(x, t) = \epsilon(x, t) \tag{16}$$

Let assume that the model error $\epsilon(x, t)$ is Gaussian, zero-mean, not correlated in the space-time domain, and described by its covariance matrix Q.

Looking for the solution $\mathbf{X}$, that solves the system of Eqs. (16, 7, 8), is rewritten again as an optimization problem. A cost function J_2 is defined and has to be minimized by controlling the two unknowns $\mathbf{X}(0)$ and $\epsilon(t)$:

$$J_2(\mathbf{X}(0), \epsilon(t)) = J_1(\mathbf{X}(0), \epsilon(t)) + \frac{1}{2}\int_A (\epsilon(\mathbf{x}, t))^T Q^{-1}(\mathbf{x}, t)\epsilon(\mathbf{x}, t) d\mathbf{x}dt \tag{17}$$

Using the adjoint variable defined by Equations (10) and (11), the gradient of J_2 is:

$$\frac{\partial J}{\partial \mathbf{X}(0)}[\mathbf{X}(0), \epsilon(t)] = \mathbb{P}^T \left(\frac{\mathbb{P}(\mathbf{X}(0)) - I_1}{B}\right) + \lambda(t_0) \tag{18}$$

$$\frac{\partial J}{\partial \epsilon(t)}[\mathbf{X}(0), \epsilon(t)] = Q^{-1}\epsilon(t) + \lambda(t) \tag{19}$$

Controlling the error term $\epsilon(t)$ allows to better estimate motion, as it will be illustrated in the results section on a synthetic experiment.

4. Results

This section is split in the same way than Section 3: first the choice of image information that has to be assimilated, in order to get optimal results, will be illustrated on satellite data. The aim is to demonstrate the improvement obtained, when adding the second observation term, on low contrast structures. Second, the impact of adding a model error in the data assimilation system will be quantified on synthetic data, as no ground truth would be available on real data to quantify this impact.

4.1 Uncertainty on image data

A sequence of four satellite images, acquired over Black Sea, in July 2005, by NOAA-AVHRR sensors, is displayed on the first row of Fig. 1. Two data assimilation methods are implemented. The first one, denoted M1, corresponds to the minimisation of J, as written in Equation (9), while, in the second one, denoted M2, an additional observation term, corresponding to $\mathbb{H}_2$ (Equation (14)), is added. Results of M1 and M2 are displayed respectively on Fig. 1, second and third rows, for the pseudo-image component, and on Fig. 2, left and right, for the initial motion fields. The impact of assimilating the gradient information may be seen on the filament structure, that is displayed in red on Fig. 3. Its real motion is displayed by blue arrows and is better assessed by the method M2.

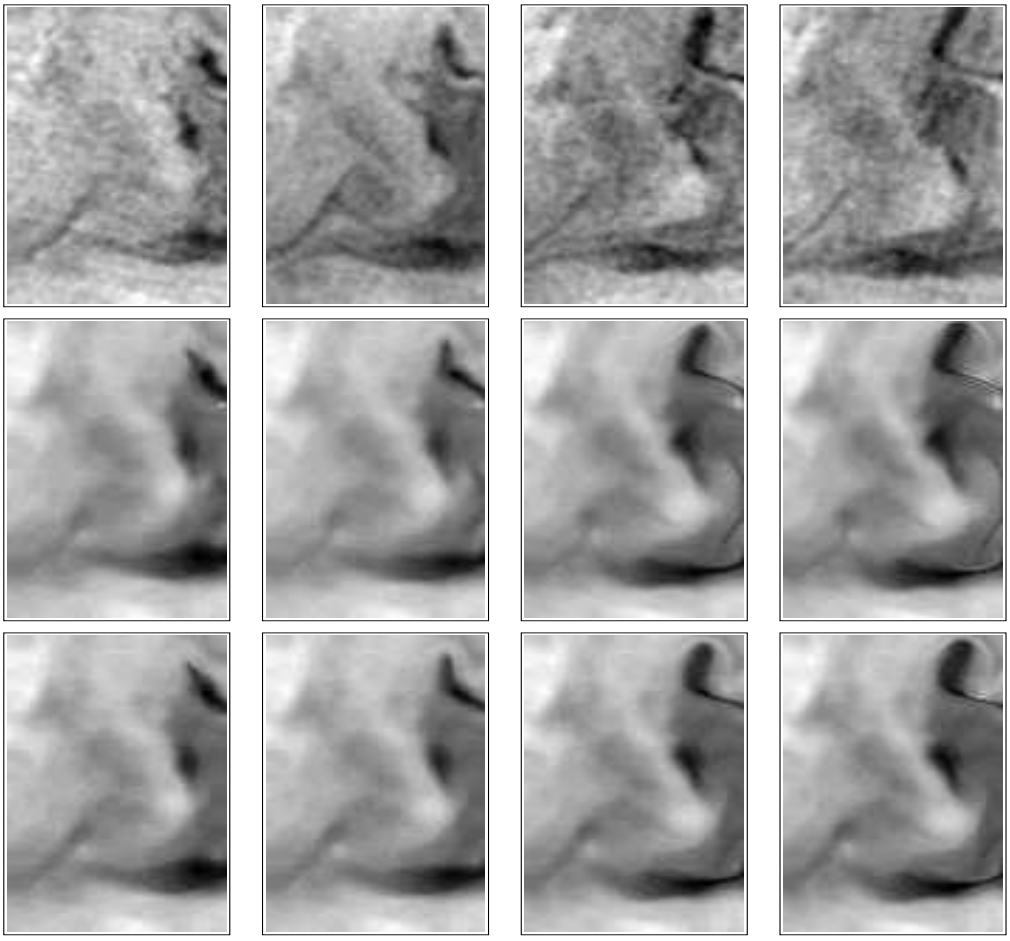

Figure 1: Up: image observation. Middle: result with M1. Down: result with M2.

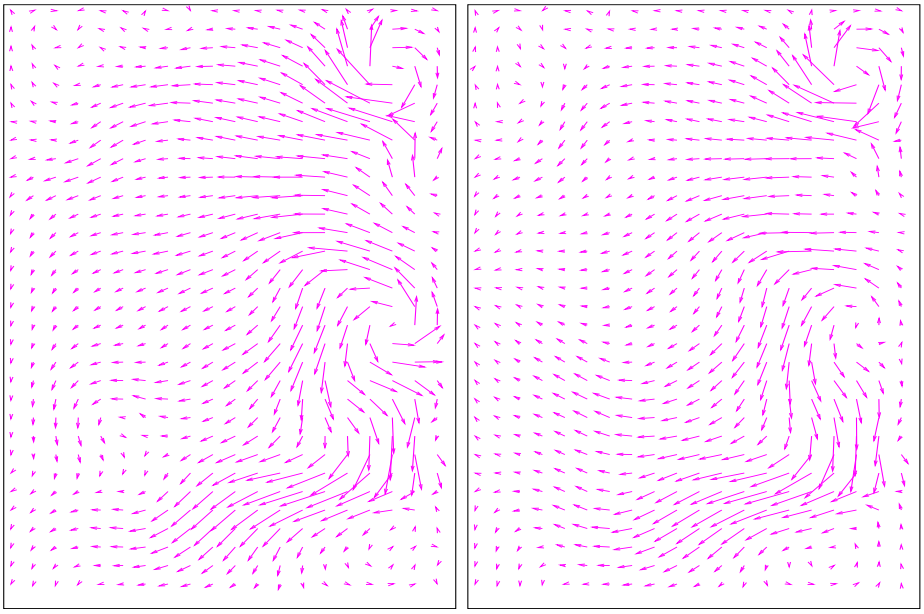

Figure 2: Left: motion field estimated by M1. Right: by M2.

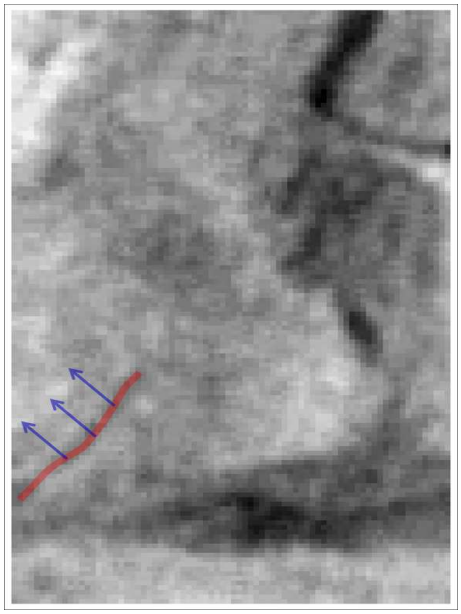

Figure 3: Location and motion of the filament on the fourth observation.

4.2 Uncertainty on evolution laws

Two algorithms are implemented and compared, in order to demonstrate and quantify the impact of the model error term. The first one is named IM, that stands for Imperfect Model, and satisfies Eqs. (16,7,8) with the error term $\epsilon(\mathbf{x}, t)$ included in the evolution equation. The second one, named PM for Perfect Model, satisfies Eqs. (4,7,8).

A synthetic experiment[1] is conducted. Given initial condition $\mathbf{X}(0)$, at time 0, displayed on Fig. 4, and given a noise function $b(\mathbf{x}, t)$, Eq. (20) is integrated in time:

$$\frac{\partial \mathbf{X}}{\partial t}(x,t) + \mathbb{M}(\mathbf{X})(x,t) = b(x,t) \quad (20)$$

$$\mathbf{X}(x,0) = \mathbf{X}(0) \quad (21)$$

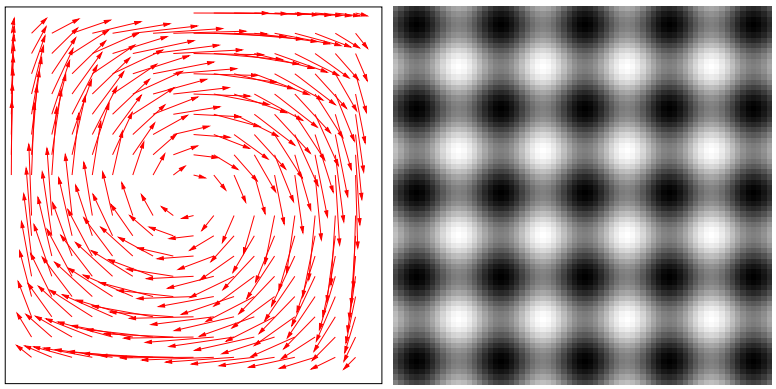

Figure 4: Condition initiale $\mathbf{w}_r(0)$ et $I_s(0)$.

In the experiment, $b(\mathbf{x}, t)$ is constant in space, and null except at one single date $t = t_N/2 = 41$. $b(\mathbf{x}, 41)$ has a null component on the pseudo-image. Its component on motion is represented on the right part of Fig. 5, where the motion component of b, at date 0, is also displayed.

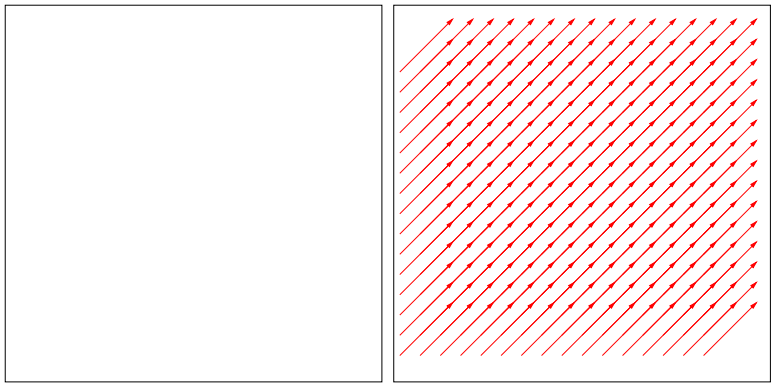

Figure 5: Motion component of noise b at dates 0 and 41.

5 snapshots of the simulation, at dates $t = 2$, 22, 42, 62, 82, are taken as observations for the assimilation process with the Imperfect and Perfect Models. They are displayed in Fig. 6. Motion obtained from the simulation and later used as ground-truth is displayed on the same figure.

[1]Thanks to Dominique Béréziat, Université Pierre et Marie Curie, 75005 Paris, France.

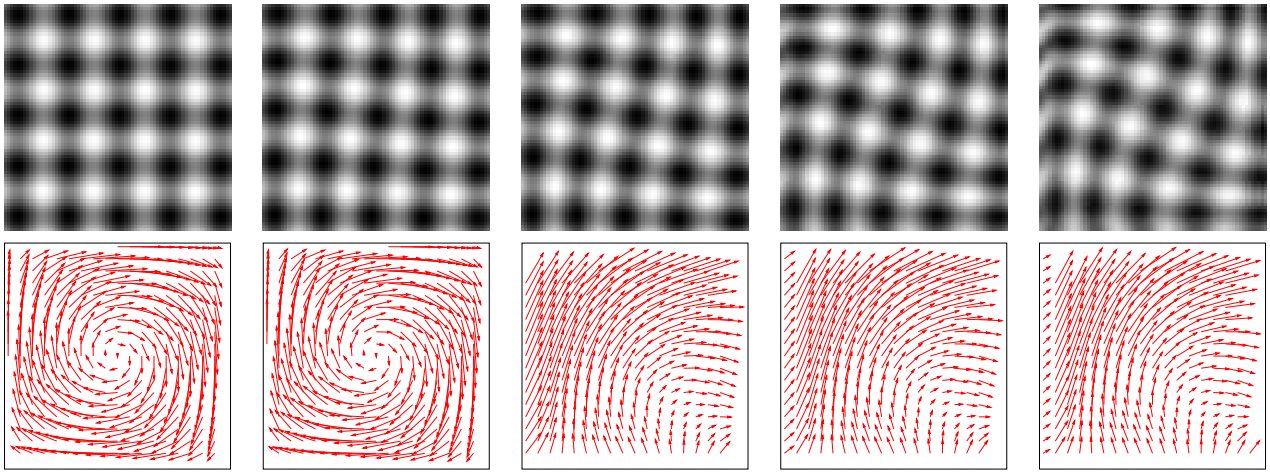

Figure 6: Up: image observations. Down: ground truth of motion at observation dates.

In order to understand the impact due to b during the simulation, the motion field, that is obtained on the last frame of the simulation, without adding b, is displayed on Fig. 7 and compared to the one obtained when adding b.

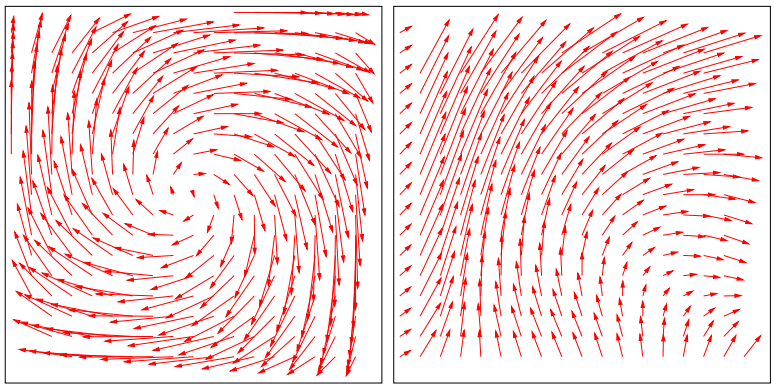

Figure 7: Left: motion obtained without b, Right: with b.

The data assimilation process is then applied with IM and PM. Results of the initial motion field are visualized on Fig. 8 and compared to the ground-truth.

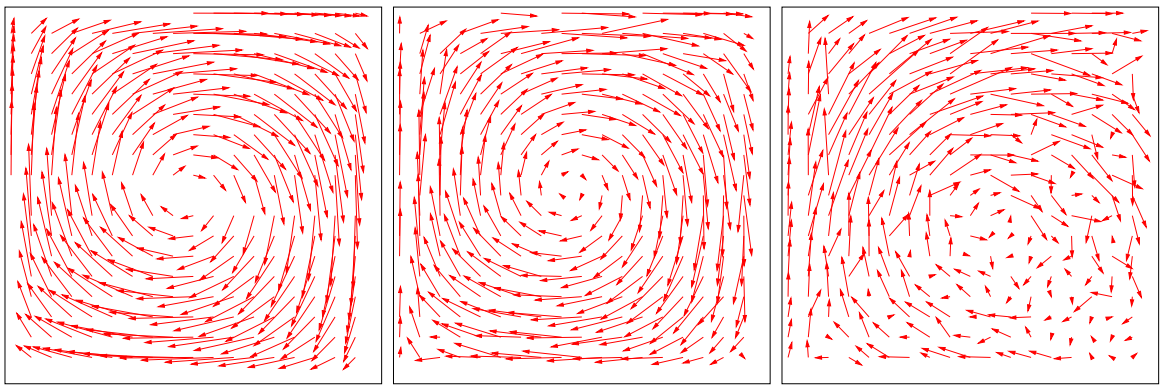

Figure 8: From left to right: ground-truth, result of IM, result of PM.

Statistics are also computed on the discrepancy between data assimilation results and ground-truth, for initial motion fields, and given in table 1. Index $\boldsymbol{r}$ concerns the ground-truth, which is the $\boldsymbol{r}$eference, while index $\boldsymbol{e}$ corresponds to the result, that is $\boldsymbol{e}$stimated with, respectively, PM on the first line, and IM on the second one. θ denotes the orientation of the

motion vector and $\|\mathbf{w}\|$ its norm. Values are given for the average and standard deviation of the orientation error. Minimum, maximum, average, and standard deviation values of the relative norm error are also provided.

		$\|\theta_r - \theta_e\|$		$\|\|\mathbf{w}_r\| - \|\mathbf{w}_e\|\|/\|\mathbf{w}_r\|$			
method	date	mean	stdev	min	max	mean	stdev
PM	$t = 0$	31.4	34.4	0.0002	7.7	0.49	0.44
IM	$t = 0$	6.0	12.1	0.00005	3.0	0.13	0.14

Table 1: Statistics on results: comparison of estimated motion $\mathbf{w}_e(0)$ with ground-truth $\mathbf{w}_r(0)$.

5. Conclusion

The paper discusses some of the uncertainties, which have to be faced when retrieving motion from image data, in order to correctly monitor ocean surface circulation on satellite acquisitions.

The first set concerns those on the data observations. Satellite acquisitions are often contaminated by noise and occluded by clouds. This has to be taken into account in the motion estimation process. As explained in the paper, dedicated observation errors are computed from the metadata documenting the satellite acquisitions: they allow not taking into account corrupted data during the estimation process. Deciding which image information has to be including in the observation vector is also mandatory to assure a good quality result. As illustration, we discuss the case of fine filaments with low contrast, which require to efficiently compute gradients and to include them in the observation data, in order to be correctly monitored.

The second type of uncertainty concerns the evolution equations of motion field and images. The full set of equations that represents the processes, which create the image sequence, is not at hand. The assumptions, that are used in the dynamic model, are a rough approximation of the reality. As described in the paper, adding a model error, in the assimilation process has a strong impact on the quality of results.

Perspectives concern two main lines of research. First refining the image information, that is assimilated, and, for instance, add structures' representation in the observation vector. Second, the weak formulation of 4D-Var will be used to monitor dynamics' errors, which are occuring during the acquisition period.

ACKNOWLEDGEMENTS

Satellite data have been provided by E. Plotnikov and G. Korotaev from the Marine Hydrophysical Institute of Sevastopol, Ukraine. Dominique Béréziat, from Université Pierre et Marie Curie, and Yann Lepoittevin, from Inria, provided some of the experimental results described in the paper.

Authors

Isabelle Herlin
Inria
B.P. 105, 78153 Le Chesnay, France

E-mail: Isabelle.Herlin@inria.fr
Telephone: +33 1 39 63 53 71

Etienne Huot
Inria
B.P. 105, 78153 Le Chesnay, France
E-mail: Etienne.Huot@inria.fr
Telephone: +33 1 39 63 58 12

References

Béréziat, D. and Herlin, I. (2011). Solving ill-posed image processing problems using data assimilation. *Numerical Algorithms*, 56(2):219–252.

Béréziat, D. and Herlin, I. (2012). Non linear observation equation for motion estimation. In *ICIP*.

Deriche, R. (1987). Using canny's criteria to derive a recursively implemented optimal edge detector. *International Journal of Computer Vision*, 1(2):167–187.

Heitz, D., Mémin, E., and Schnörr, C. (2010). Variational fluid flow measurements from image sequences: synopsis and perspectives. *Experiments in Fluids*, 48(3):369–393.

Herlin, I., Béréziat, D., and Mercier, N. (2011). Recovering missing data on satellite images. In *SCIA*, pages 697–707.

Herlin, I., Béréziat, D., and Mercier, N. (2012). Improvement of motion estimation by assessing the errors on the evolution equation. In *VISAPP (2)*, pages 235–240.

Horn, B. and Schunk, B. (1981). Determining optical flow. *Artificial Intelligence*, 17:185–203.

Le Dimet, F.-X. and Talagrand, O. (1986). Variational algorithms for analysis and assimilation of meteorological observations: Theoretical aspects. *Tellus*, 38A:97–110.

Papadakis, N., Corpetti, T., and Mémin, E. (2007). Dynamically consistent optical flow estimation. In *ICCV*, pages 1–7.

Titaud, O., Vidard, A., Souopgui, I., and Le Dimet, F.-X. (2010). Assimilation of image sequences in numerical models. *Tellus A*, 62:30–47.

Trémolet, Y. (2006). Accounting for an imperfect model in 4D-Var. *Quaterly Journal of the Royal Meteorological Society*, 132(621):2483–2504.

Valur Hólm, E. (2008). Lectures notes on assimilation algorithms. European Centre for Medium-Range Weather Forecasts Reading.

Zhu, C., Byrd, R., Lu, P., and Nocedal, J. (1997). L-bfgs-B: Algorithm 778: L-bfgs-B, FORTRAN routines for large scale bound constrained optimization. *ACM Transactions on Mathematical Software*, 23(4):550–560.